INTRODUCTION

This material is intended to supply the reader with sample locations (Fig. 1), mineral assemblages (Table 1), microprobe results (Fig. 2, Tables 2-8), and phase diagrams (Figs. 3-10; Tables 9-14) used in the estimation of conditions of Jurassic metamorphism in the central Ruby Mountains, Nevada (Hudec, 1992). In addition, a discussion of these results is presented. It is hoped that the presentation of the data will assist future workers in recalculating metamorphic conditions using other techniques or more accurate thermodynamic properties.

ANALYTICAL METHODS

Over 175 thin sections from the central Ruby Mountains were prepared as part of a multidisciplinary study involving field mapping, microstructural analysis, isotopic dating, and thermobarometry. Rock types examined include schist, impure marble, quartzite, granite, amphibolite, and hornblende-biotite quartz diorite. After detailed study of the fabrics and mineral assemblages, polished sections were prepared from seven samples (six pelitic schists and one garnet amphibolite, Table 1) for

microprobe analysis. These samples were chosen primarily on the basis of their comparatively unaltered states, good equilibrium textures, and possession of low-variance mineral assemblages. In addition, an effort was made to include as wide a range of schist bulk compositions as possible.

In each polished section all variable-composition minerals (muscovite, biotite, plagioclase feldspar, garnet, cordierite, and staurolite in schist; garnet, plagioclase, and hornblende in garnet amphibolite) were analyzed using an electron microprobe. The probe results were then entered into the software package GEO-CALC (Berman and others, 1985; Perkins and others, 1986), which is designed to calculate phase diagrams incorporating all possible reactions between the phases present in any given sample, using mineral compositions derived from microprobe analyses.

GEO-CALC requires individual probe analyses as input, so that for each sample a "typical" probe analysis was selected for each mineral composition entered into the program. After the first phase diagram was generated, successive iterations used different mineral analyses in an effort to fine-tune the results and achieve better definition of the cluster of invariant points. In practice this procedure worked much better on diagrams with

fewer than 30 curves; beyond that point a change in mineral compositions designed to bring one invariant point into the cluster usually caused several others to move out.

The process of defining a "best" cluster is obviously somewhat subjective, but appears to have little effect on the final result. Varying the mineral compositions can increase or decrease the tightness of the cluster, but its absolute position in P-T space remains relatively unchanged.

RESULTS

SEQUENCE OF METAMORPHIC EVENTS

M_1 - The peak of the first phase of regional metamorphism (M_1) is recorded in schist by porphyroblasts of staurolite, local andalusite, and probably also the cores of garnet crystals. These phases grew discordantly across the first foliation in the rocks (S_1), but prior to the later stages of D_2 deformation. This distinguishes them from M_2 porphyroblasts, which are interpreted to have grown during late-D_2, D_3, and post-D_3 time.

In addition to microstructural arguments, many samples show mineralogical and textural evidence that staurolite, andalusite, and garnet cores did not grow

during M_2. The aluminosilicate that grew during M_2 was sillimanite, which is intergrown with M_2 biotite, muscovite, and quartz, and shows the syn- to post-kinematic fabric characteristic of all other M_2 minerals. Andalusite must therefore have grown at lower temperatures than were present during M_2, and its survival in a comparatively unaltered state probably reflects the small free energy change involved in the andalusite-sillimanite transition.

Staurolite porphyroblasts are commonly anhedral, and are typically partially to completely replaced by a nearly monomineralic aggregates of coarse-grained muscovite porphyroblasts. Like sillimanite, these muscovite porphyroblasts can be either aligned parallel to S_2 or randomly oriented, again consistent with the syn-S_2 to post- kinematic timing of M_2. The breakdown of staurolite to muscovite is therefore interpreted to have occurred during prograde M_2 metamorphism, and staurolite is therefore interpreted to be pre-M_2.

Many garnets examined in this study have inclusion-rich (primarily quartz) cores and inclusion-free rims, interpreted as having grown during M_1 and M_2 respectively. Microprobe line scans of garnet commonly show a slight break in composition across the inclusion-rich/inclusion-free boundary (Fig. 2), with higher temperature (more

iron-rich) compositions in the rim zone. A garnet profile of this type could conceivably have formed during a single prolonged period of garnet growth, but the fact that the change in composition is accompanied by a very distinct change in texture argues for a polyphase history. Garnet cores are therefore interpreted to have grown during M_1, consistent with the observation that they locally contain the planar inclusion trails typical of other M_1 porphyroblasts.

M_2 - M_2 was most likely a higher temperature event than M_1, as sillimanite replaced andalusite as the stable aluminosilicate phase. Schists typically contain the M_2 assemblage quartz-muscovite-biotite-plagioclase-sillimanite $\pm$ garnet $\pm$ cordierite, with accessory zircon, apatite, and tourmaline (Table 1). The only garnet amphibolite examined in the study contains the M_2 assemblage quartz-hornblende-garnet- plagioclase-sphene.

Study of fabrics with respect to M_2 minerals shows that M_2 began in late D_2 time, continued through D_3, and ended some time after the cessation of deformation. In any given thin section most of the M_2 minerals grew syn-kinematic to D_2, but there are usually some post-kinematic muscovite and biotite porphyroblasts growing at high angles to the foliation. Microprobe analyses (Tables 2, 3)

indicate that post-kinematic micas are essentially identical to syn-kinematic micas in composition, so muscovite and biotite porphyroblasts are interpreted to have grown during the final stages of M_2 rather than during some later event. In most of the study area there was no significant mineral growth following M_2. Exceptions to this include rocks involved in the Ruby- East Humboldt mylonitic shear zone on the extreme west edge of the range, rocks in the contact aureole of the Oligocene Harrison Pass pluton, and rocks that have undergone variable amounts of retrogression during weathering. None of the samples from which polished sections were made show any evidence of post-M_2 mineral growth.

Staurolite is included in the thermobarometric calculations for M_2 presented below even though it is not an M_2 phase, because it was participant in M_2 reactions and was therefore in equilibrium with a number of M_2 phases. Guidotti (1968) suggested that the prograde breakdown of staurolite to muscovite could be caused by the reaction:

staur + Na-mus + qtz = sill + bio + K-mus + Ab + gar + H_2O

which marks the transition from lower to upper sillimanite zone. This reaction would account for the observation that in many thin sections sillimanite is concentrated near the remnants of staurolite porphyroblasts. Further-

more, because the reaction is a major sink for quartz, it might also explain the lack of quartz inclusions in M_2 garnet rims.

In a few instances small amounts of cordierite were observed around the edge of muscovites pseudomorphing staurolite, indicating that the reaction:

bio (ss) + qtz + staur = mus + cord (ss) + H_2O (ss) = solid solution

may have been important in some samples.

THERMOBAROMETRY

Microprobe analyses for muscovite, biotite, garnet, plagioclase, cordierite, staurolite, and hornblende are displayed in tables 2-8. These mineral compositions were used to generate phase diagrams (Figs. 3-9), each of which is discussed separately below. The lists of reactions for the phase diagrams are contained in tables 9-14.

Sample RM 1 contains the complete M_2 mineral assemblage (Table 1), and therefore has the greatest number of reaction curves (92) of any of the samples studied (Table 9, Fig. 3). The majority of the invariant points fall in a very well-defined cluster at 4.0-4.7 kb and 560-625°C.

A number of curves do not pass through this region, most notably the garnet-biotite geothermometer (curve #80), which indicates temperatures of 675-690°C. It is possible to move this curve into the cluster region by selecting the most magnesian biotite and most ferrous garnet from the probe data, but this results in a considerable loss in resolution as these compositional changes cause many invariant points that currently lie within the cluster to move elsewhere. An anomalously high garnet-biotite temperature is also a problem in sample RM 6 (curve # 76, Fig. 8), although in that sample the cluster as a whole is much less well defined. One possible explanation is that the garnet - biotite thermometer records an earlier, higher-temperature part of the cooling history, but a number of reaction curves involving garnet and biotite pass through the cluster area, and it seems unlikely that garnet and biotite would stop reacting with each other while they were both continuing to react with other mineral phases. The anomalously high garnet-biotite temperatures therefore remain unexplained.

Sample RM 2 contains the tightest cluster of invariant points of any of the samples, and indicates metamorphic conditions of 4.0-4.4 kb and 570-600°C (Fig. 4, Table 10). Unlike sample RM 1, RM 2 is displayed showing only curves involving Fe-cordierite; the Mg-

cordierite curves have been omitted. GEO-CALC permits calculations to be made using activities for either or both cordierite end members, and for an intermediate composition the two sets of curves generated by these activities should ideally be coincident. In actuality, the thermodynamic properties of cordierite are not very well known, and the cordierite and Fe-cordierite curves can differ by several kilobars. This is particularly true in garnet-free samples. In such a situation it is necessary to chose which end member should be included in the phase diagram. Fe-cordierite was chosen in sample RM 2 because (1) invariant points in the Mg-cordierite phase diagram do not form a cluster, (2) cordierites in this sample are relatively iron-rich (Table 6),and (3) the Fe- cordierite phase diagram produces results consistent with the rest of the samples (Fig. 10).

Invariant points in sample RM 3 do not define a cluster (Fig. 5, Table 11), and therefore do not give a reliable estimate of pressure and temperature during M_2. The intersection between the garnet-biotite geothermometer and the reaction sill + qtz + gross = anorth, widely used as an indicator of P-T conditions (e.g., Hodges and Royden, 1984), occurs at roughly 4.75 kb and 635^{o}C, but this intersection is at a very acute angle, and small shifts in the compositions of the phases involved can move

the crossing anywhere within the range 0 to 6 kb. The position of the garnet-biotite geothermometer itself is less susceptible to compositional variability, and falls in the range 600-650°C for all biotite and garnet combinations in the sample. As discussed above, however, there is some evidence that this geothermometer yields systematically high temperatures in the central Ruby Mountains, so caution is advised in using this figure as an estimate of metamorphic temperatures.

Reactions between the phases in sample RM 4 come together in a single invariant point (Fig. 6, Table 12), so there is no way to use the positions of invariant points relative to one another as a check on the reliability of the result. As an alternate method, various combinations of extreme mineral compositions were entered into the GEO-CALC program in an effort to offset the position of the reactions by the maximum amounts, and all of the resultant invariant points fell in the area outlined in Figure 6. This region is therefore considered a reasonable estimate of the conditions of M_2 metamorphism in this sample. Mg-cordierite was chosen as the cordierite phase in this assemblage because (1) the cordierites in sample RM 4 are considerably more magnesian than in sample RM 2 (Table 6), and (2) invariant points involving the reaction curve for the breakdown of Fe-

cordierite in the presence of muscovite are located at pressures of 4.8-5.8 kb, too high to be consistent with the pressures observed in other samples.

Sample RM 5 contains the same mineral assemblage as RM 2, the topologies of the resultant phase diagrams are therefore identical (Figs. 4, 7, Table 13). The cluster of invariant points in RM 5 is not as tight as RM 2, but is centered on roughly the same point and is considered a good estimate of the P-T conditions of M_2. Fe-cordierite was chosen over Mg-cordierite for the same reasons as those outlined above for sample RM 2.

Like sample RM 1, sample RM 6 contains all of the M_2 phases that have been observed in schists in the central Ruby Mountains, and therefore has a fairly complicated phase diagram (Fig. 8, Table 14). The cluster of invariant points is not nearly as well defined as in sample RM 1, and it could be argued that the points do not really define an area in P-T space at all. Most of the major invariant points lie within the region outlined in Figure 8, consistent with the P-T conditions of metamorphism as defined in the rest of the samples (Fig. 10). The phase diagram for sample RM 6 does yield very broad limits on the conditions of M_2, but it does not provide as precise an estimate as the other samples.

The phases present in sample RM 7 are related by only one reaction (Fig. 9), and thus do not yield a P-T estimate. In addition, the thermodynamic properties of hornblende are extremely poorly known, and in order to enter the data into GEO-CALC it was necessary to treat hornblende as a tremolite with very low activity (a[Mg] = 0.001-0.005). Given these limitations, the fact that reaction curve lies at somewhat higher temperatures than are indicated by the schist samples is not considered to be particularly significant. The analyses from sample RM 7 are included here primarily so that future workers can have access to the data once solution models for hornblende have been developed.

REFERENCES

Berman, R.G., Brown, T.H., and Greenwood, H.J., 1985, An internally consistent thermodynamic data base for minerals in the system Na_2O-K_2O-CaO-MgO-FeO-Fe_2O_3-Al_2O_3-SiO_2-TiO_2-H_2O-CO_2: Atomic Energy of Canada Ltd. Technical Report 377, 62p.

Guidotti, C.V., 1968, Prograde muscovite pseudomorphs after staurolite in the Rangely-Oquossoc areas, Maine: The American Mineralogists, v.53,p. 1368-1376.

Hodges, K.V., and Royden, L., 1984, Geologic thermobarometry of retrograded metamorphic rocks: an indication of the uplift trajectory of a portion of the northern Scandinavian Caledonides: Journal of Geophysical Research, V.89, No.B8, p. 7077-7090.

Hudec, M.R., 1992, Mesozoic structural and metamorphic history of the central Ruby Mountains metamorphic core complex, Nevada: Geological Society of American Bulletin, p. ???.

Perkins, E.H., Brown, T.H., and Berman, R.G., 1986, PTX-SYSTEM: three programs which calculate pressure-

temperature-composition phase diagrams: Computers and Geosciences, v. 12, p. 749-755.

Table 1

Mineral Assemblages of Thermobarometry Samples

Sample	Assemblage
RM 1	quartz-muscovite-biotite-plagioclase-sillimanite-garnet-cordierite-staurolite
RM 2	quartz-muscovite-biotite-plagioclase-sillimanite-cordierite-staurolite
RM 3	quartz-muscovite-biotite-plagioclase-sillimanite-garnet
RM 4	quartz-muscovite-biotite-plagioclase-sillimanite-cordierite
RM 5	quartz-muscovite-biotite-plagioclase-sillimanite-cordierite-staurolite
RM 6	quartz-muscovite-biotite-plagioclase-sillimanite-garnet-cordierite-staurolite
RM 7	quartz-plagioclase-garnet-hornblende-sphene

Table 2 - Microprobe Analyses of Muscovite

Sample	RM 1	RM 2	RM 2*	RM 3	RM 4	RM 5	RM 6
Na2O	1.25	1.79	1.73	1.57	1.19	1.51	1.38
K2O	9.21	8.51	8.41	8.38	9.39	8.81	9.18
MnO	0.52	0.02	0.00	0.00	0.00	0.00	0.00
MgO	0.56	0.42	0.51	0.40	0.66	0.46	0.46
CaO	0.00	0.00	0.00	0.00	0.00	0.00	0.00
FeO	1.34	0.71	0.88	1.49	3.08	1.01	1.44
Al2O3	36.32	36.94	37.33	36.59	34.90	37.14	36.76
TiO2	0.60	0.42	0.68	0.30	0.37	0.48	0.40
SiO2	46.24	46.69	46.51	46.15	46.67	46.89	46.55
H2O	4.55	4.59	4.59	4.53	4.52	4.60	4.57
sum	100.59	100.09	100.64	99.41	100.78	100.90	100.74
			Number of Ions on the Basis of 24 Oxygen				
S	6.09	6.12	6.07	6.11	6.18	6.11	6.10
Al	1.91	1.88	1.93	1.89	1.82	1.89	1.90
sum	8.00	8.00	8.00	8.00	8.00	8.00	8.00
Al	3.72	3.84	3.81	3.82	3.63	3.82	3.79
Ti	0.06	0.04	0.07	0.03	0.04	0.05	0.04
Fe	0.15	0.08	0.10	0.17	0.34	0.11	0.16
Mn	0.06	0.00	0.00	0.00	0.00	0.00	0.00
Mg	0.11	0.08	0.10	0.08	0.13	0.09	0.09
sum	4.10	4.04	4.07	4.09	4.14	4.06	4.07
Ca	0.00	0.00	0.00	0.00	0.00	0.00	0.00
K	1.55	1.42	1.40	1.42	1.53	1.47	1.54
Na	0.32	0.46	0.44	0.40	0.31	0.38	0.35
sum	1.87	1.88	1.84	1.82	1.83	1.85	1.89
OH	4.00	4.00	4.00	4.00	4.00	4.00	4.00

* This analysis is from a post-tectonic muscovite porphyroblast, and is included for comparison to the sample to its left, which is in the foliation.

Table 3 - Microprobe Analyses of Biotite

Sample	RM 1	RM 2	RM 3	RM 4	RM 5	RM 6	RM 6*
Na2O	0.18	0.27	0.27	0.33	0.37	0.27	0.25
K2O	8.79	8.65	8.62	9.32	8.64	8.44	8.81
MnO	0.16	0.05	0.14	0.20	0.13	0.20	0.14
MgO	8.49	8.75	8.42	12.35	8.28	9.02	9.07
CaO	0.00	0.00	0.02	0.00	0.00	0.01	0.00
FeO	22.18	21.22	20.88	16.50	21.27	19.71	19.68
Al2O3	19.38	20.23	19.88	19.69	19.99	19.93	19.93
TiO2	1.86	1.90	1.75	1.51	2.23	1.78	1.81
SiO2	35.16	35.94	35.62	36.51	35.28	36.13	35.43
H2O	3.94	4.01	3.95	4.05	3.96	3.97	3.94
sum	100.14	101.02	99.55	100.46	100.15	99.46	99.06
			Number of Ions on the Basis of 24 Oxygen				
Si	5.35	5.37	5.41	5.40	5.34	5.45	5.38
Al	2.65	2.63	2.59	2.60	2.66	2.55	2.62
sum	8.00	8.00	8.00	8.00	8.00	8.00	8.00
Al	0.83	0.94	0.96	0.83	0.90	0.99	0.95
Ti	0.21	0.21	0.20	0.17	0.25	0.20	0.21
Fe	2.82	2.65	2.65	2.04	2.69	2.48	2.50
Mn	0.02	0.01	0.02	0.03	0.02	0.03	0.02
Mg	1.93	1.95	1.91	2.72	1.87	2.03	2.05
sum	5.81	5.76	5.74	5.79	5.73	5.73	5.73
Ca	0.00	0.00	0.00	0.00	0.00	0.00	0.00
K	1.71	1.65	1.67	1.76	1.67	1.62	1.71
Na	0.05	0.08	0.08	0.09	0.11	0.08	0.07
sum	1.76	1.73	1.75	1.85	1.78	1.71	1.78
OH	4.00	4.00	4.00	4.00	4.00	4.00	4.00

* This analysis is from a syn-tectonic biotite, and is included for comparison to the sample to its left, which is post-tectonic.

Table 4

Microprobe Analyses of Garnet

Sample	RM 1	RM 3	RM 6	RM 7
MgO	2.32	2.48	2.36	0.60
CaO	1.53	0.59	1.33	14.70
MnO	6.29	4.24	7.04	7.24
Al2O3	20.82	20.91	20.81	20.40
TiO2	0.00	0.00	0.02	-
FeO	32.61	34.97	31.23	19.35
Fe2O3	0.30	0.31	0.25	1.68
SiO2	36.57	37.34	37.14	36.98
sum	100.44	100.84	100.18	100.95

Number of Ions on the Basis of 24 Oxygen

Si	5.93	6.00	6.01	5.88
Al	0.07	0.00	0.00	0.12
sum	6.00	6.00	6.00	6.00
Al	3.91	3.96	3.97	3.71
Fe+3	0.04	0.04	0.03	0.20
Ti	0.00	0.00	0.00	-
sum	3.95	4.00	4.00	3.91
Mg	0.56	0.59	0.57	0.14
Fe+2	4.52	4.70	4.22	3.82
Mn	0.86	0.58	0.96	0.97
Ca	0.27	0.10	0.23	2.51
sum	6.21	5.98	5.99	7.45
Almandine	72.32	78.68	70.54	41.55
Pyrope	9.19	9.93	9.52	2.28
Spessartine	14.13	9.67	16.11	15.74
Grossular	3.47	0.77	3.04	35.56
Andradite	0.89	0.94	0.79	4.87

Table 5 - Microprobe Analyses of Plagioclase

Sample	RM 1	RM 2	RM 3	RM 4	RM 5	RM 6	RM 7
Na2O	9.35	10.71	10.73	8.99	0.34	8.72	0.71
Al2O3	23.22	22.00	22.08	24.40	22.25	23.88	35.87
SiO2	63.13	65.24	66.42	62.27	66.44	62.87	45.05
K2O	0.07	0.05	0.09	0.05	0.06	0.07	0.04
CaO	4.26	1.68	1.42	4.40	1.87	4.40	18.67
Fe2O3	0.23	0.11	0.00	0.01	0.00	0.09	0.53
sum	100.26	99.79	100.74	100.12	100.96	100.03	100.87

Number of Ions on the Basis of 8 Oxygen

Na	0.80	0.91	0.91	0.77	0.87	0.75	0.06
Al	1.21	1.14	1.13	1.27	1.14	1.24	1.93
Si	2.79	2.87	2.89	2.75	2.89	2.77	2.06
K	0.00	0.00	0.00	0.00	0.00	0.00	0.00
Ca	0.20	0.08	0.07	0.21	0.09	0.21	0.92
Fe+3	0.01	0.00	0.00	0.00	0.00	0.00	0.02
Ab	79.61	91.75	92.72	78.50	90.58	77.86	10.54
Or	0.37	0.30	0.49	0.27	0.36	0.43	0.10
An	20.02	7.95	6.80	21.23	9.06	21.70	89.35

Table 6

Microprobe Analyses of Cordierite

Sample	RM 1	RM 2	RM 4	RM 5	RM 6
FeO	8.35	8.93	6.36	9.58	7.85
CaO	0.03	0.00	0.04	0.00	0.05
MgO	6.49	6.03	8.82	6.21	6.52
MnO	0.47	0.30	0.50	0.35	0.47
Al2O3	33.35	33.37	33.97	33.47	33.80
SiO2	47.09	47.28	48.28	47.08	47.45
sum	95.78	95.91	97.97	96.69	96.14
Number of Ions on the Basis of 18 Oxygen					
Si	4.98	5.00	4.95	4.96	4.98
Al	1.02	1.00	1.05	1.04	1.02
sum	6.00	6.00	6.00	6.00	6.00
Al	3.13	3.16	3.05	3.11	3.17
Fe	0.74	0.79	0.55	0.84	0.69
Mg	1.02	0.95	1.37	0.97	1.02
Mn	0.04	0.03	0.04	0.03	0.04
Ca	0.00	0.00	0.00	0.00	0.01
XMg	0.57	0.54	0.70	0.53	0.58

Table 7

Microprobe Analyses of Staurolite

Sample	RM 1	RM 2	RM 5	RM 6
MgO	1.39	1.05	1.38	1.13
CaO	0.01	0.01	0.00	0.00
MnO	0.36	0.56	0.27	0.50
Al2O3	54.89	57.10	56.13	55.66
TiO2	0.48	0.44	0.37	0.55
FeO	13.05	12.46	13.91	12.97
SiO2	27.61	26.22	27.47	27.55
ZnO	0.55	0.55	0.25	0.92
H2O	2.17	2.17	2.20	2.19
sum	100.51	100.56	101.98	101.47

Number of Ions on the Basis of 24 Oxygen

Si	3.81	3.61	3.77	3.77
Al	8.93	9.27	9.01	8.98
Ti	0.05	0.05	0.04	0.06
sum	8.98	9.32	9.05	9.04
Mg	0.29	0.22	0.28	0.23
Fe	1.51	1.44	1.58	1.48
Zn	0.06	0.06	0.02	0.09
Mn	0.04	0.07	0.03	0.06
Ca	0.00	0.00	0.00	0.00
sum	1.89	1.77	1.92	1.87
OH	1.00	1.00	1.00	1.00
XFe	0.80	0.81	0.83	0.80

Table 8

Microprobe Analyses of Hornblende

Sample	RM 7-1	RM 7-2	RM 7-3	RM 7-4
Na2O	0.63	0.83	0.80	0.77
K2O	0.22	0.31	0.27	0.30
MnO	0.65	0.61	0.63	0.58
MgO	7.98	6.49	7.03	6.43
CaO	12.39	12.65	12.65	12.63
FeO	21.75	22.20	22.36	22.88
Al2O3	8.01	11.51	10.12	11.27
TiO2	0.28	0.41	0.35	0.37
SiO2	46.70	43.94	45.10	44.24
H2O	1.99	1.98	1.99	1.99
sum	100.60	100.93	101.30	101.46
Number of Ions on the Basis of 24 Oxygen				
Si	7.04	6.64	6.79	6.67
Al	0.96	1.36	1.21	1.33
sum	8.00	8.00	8.00	8.00
Al	0.46	0.69	0.58	0.67
Ti	0.03	0.05	0.04	0.04
Fe	2.74	2.81	2.81	2.88
Mg	1.79	1.46	1.58	1.44
Mn	0.08	0.08	0.08	0.07
sum	5.11	5.09	5.09	5.11
Na	0.18	0.24	0.23	0.22
Ca	2.00	2.05	2.04	2.04
K	0.04	0.06	0.05	0.06
sum	2.23	2.35	2.32	2.32
OH	1.00	1.00	1.00	1.00

Table 9

Reaction List for Sample RM 1

Assemblages on the left are stable on the:
high side of the Y-axis variable, or the
high side of the X-axis variable for vertical reactions

1): 2 Alm + 4 Pg + 9 aQz = 4 W + 3 fCd + 4 Ab
2): 2 Ann + 8 Pg + 15 aQz = 8 W + 2 Ms + 3 fCd + 8 Ab
3): Gr + 2 Pg + 3 aQz = 2 W + 3 An + 2 Ab
4): 8 Pg + 2 Phl + 15 aQz = 8 W + 2 Ms + 3 Cd + 8 Ab
5): 4 Pg + 2 Py + 9 aQz = 4 W + 3 Cd + 4 Ab
6): aQz + Pg = Ab + Si + W
7): 4 Alm + 2 Ms + 3 aQz = 3 fCd + 2 Ann
8): 2 W + 3 Ms + 5 Alm + 2 Ab = 3 Ann + 3 fCd + 2 Pg
9): 3 aQz + 2 Pg + Ann = 2 Ab + Alm + Ms + 2 W
10): 2 Alm + 6 An + 3 aQz = 2 Gr + 3
11): 3 fCd + 3 Gr + 2 Pg = 2 W + 9 An + 2 Alm + 2 Ab
12): 3 Cd + 2 Alm = 3 fCd + 2 Py
13): 4 Si + 5 aQz + 2 Alm = 3 fCd
14): 5 W + 9 Si + 2 Alm + 5 Ab = 3 fCd + 5 Pg
15): 8 Ab + 6 Alm + 37 aQz + 4 St = 8 Pg + 17 fCd
16): 110 Pg + 21 fCd + 10 Alm = 110 Ab + 18 St + 74 W
17): 10 Alm + 55 aQz + 4 St = 8 W + 23 fCd
18): 3 fCd + 4 Gr + 2 Ms = 3 aQz + 12 An + 2 Ann
19): 3 fCd + 5 Gr + 2 Ms + 2 Pg = 2 W + 15 An + 2 Ann + 2 Ab
20): 3 Cd + 2 Ann = 3 fCd + 2 Phl
21): 3 aQz + 4 Py + 2 Ms + 3 fCd = 2 Ann + 6 Cd
22): 8 Si + 7 aQz + 2 Ann = 3 fCd + 2 Ms
23): 3 fCd + 2 Ms + 7 Pg = 7 W + 15 Si + 2 Ann + 7 Ab
24): 10 Ann + 95 aQz + 8 St = 16 W + 10 Ms + 31 fCd
25): 3 Cd + 4 Gr + 2 Ms = 3 aQz + 2 Phl + 12 An
26): 6 An + 2 Py + 3 aQz = 2 Gr + 3 Cd
27): 3 Cd + 3 Gr + 2 Pg = 2 W + 2 Py + 9 An + 2 Ab
28): 2 Si + aQz + Gr = 3 An
29): W + 3 Si + Gr + Ab = 3 An + Pg
30): 5 Gr + 20 aQz + 2 St = 4 W + 4 fCd + 15 An
31): 3 aQz + 4 Py + 2 Ms = 3 Cd + 2 Phl
32): 8 Si + 7 aQz + 2 Phl = 3 Cd + 2 Ms
33): 3 Cd + 2 Ms + 7 Pg = 7 W + 15 Si + 2 Phl + 7 Ab
34): 10 Phl + 95 aQz + 8 St = 16 W + 10 Ms + 16 fCd + 15 Cd
35): 4 Si + 5 aQz + 2 Py = 3 Cd
36): 5 W + 9 Si + 2 Py + 5 Ab = 3 Cd + 5 Pg
37): 8 Ab + 6 Py + 37 aQz + 4 St = 8 Pg + 8 fCd + 9 Cd
38): 10 Py + 110 Pg + 36 fCd = 110 Ab + 15 Cd + 18 St + 74 W
39): 10 Py + 55 aQz + 4 St = 8 W + 8 fCd + 15 Cd

Table 9 (continued)

40): 4 Ab + 11 aQz + 2 St = 6 Si + 4 Pg + 4 fCd
41): 4 fCd + 15 Pg = 11 W + 2 St + 5 Si + 15 Ab
42): 15 aQz + 2 St = 4 W + 10 Si + 4 fCd
43): Alm + Gr + Ms = 3 An + Ann
44): 7 Alm + 5 Ms = 6 Si + 3 fCd + 5 Ann
45): Alm + Ms = 2 Si + aQz + Ann
46): Alm + Ms + Pg = W + 3 Si + Ann + Ab
47): 12 Pg + 37 Ms + 65 Alm = 12 Ab + 37 Ann + 30 fCd + 6 St
48): 12 W + 55 Ms + 95 Alm = 55 Ann + 48 fCd + 6 St
49): 12 W + 23 Ms + 31 Alm = 23 Ann + 48 aQz + 6 St
50): 6 Si + 5 Gr + 3 fCd = 2 Alm + 15 An
51): 12 Ab + 30 fCd + 37 Gr + 6 St = 12 Pg + 111 An + 28 Alm
52): 48 fCd + 55 Gr + 6 St = 12 W + 165 An + 40 Alm
53): 20 W + 6 St + 7 Gr + 32 Ab = 8 Alm + 21 An + 32 Pg
54): 23 Gr + 48 aQz + 6 St = 12 W + 69 An + 8 Alm
55): 24 Ab + 34 Py + 111 aQz + 12 St = 24 Pg + 51 Cd + 16 Alm
56): 46 Py + 165 aQz + 12 St = 24 W + 69 Cd + 16 Alm
57): 74 Si + 20 Pg + 22 Alm = 20 Ab + 13 fCd + 10 St
58): 12 Ab + 13 aQz + 6 St = 34 Si + 12 Pg + 8 Alm
59): 4 W + 22 Si + 6 Alm = 5 fCd + 2 St
60): 21 Si + 25 Pg + 8 Alm = 25 Ab + 6 St + 13 W
61): 25 aQz + 6 St = 12 W + 46 Si + 8 Alm
62): 6 Si + 2 Ms + 7 Gr + 3 fCd = 2 Ann + 21 An
63): 12 Ab + 30 fCd + 65 Gr + 28 Ms + 6 St = 12 Pg + 195 An + 28 Ann
64): 48 fCd + 95 Gr + 40 Ms + 6 St = 12 W + 285 An + 40 Ann
65): 2 Ann + 2 Ms + 4 Py + 3 aQz = 4 Phl + 3 fCd
66): 14 Py + 10 Ms + 15 fCd = 10 Ann + 21 Cd + 12 Si
67): 28 Ab + 5 fCd + 22 Ms + 14 St = 130 Si + 28 Pg + 22 Ann
68): 17 fCd + 30 Ms + 14 St = 28 W + 190 Si + 30 Ann
69): Py + Ms + Gr = 3 An + Phl
70): 3 Cd + 7 Gr + 2 Ms + 6 Si = 2 Phl + 21 An
71): 3 Cd + 5 Gr + 6 Si = 2 Py + 15 An
72): 12 Ab + 42 Cd + 37 Gr + 6 St = 28 Py + 12 Pg + 12 fCd + 111 An
73): 60 Cd + 55 Gr + 6 St = 12 W + 40 Py + 12 fCd + 165 An
74): 28 Si + 4 Pg + 11 Gr + 4 fCd = 4 Ab + 33 An + 2 St
75): 7 Py + 5 Ms = 3 Cd + 5 Phl + 6 Si
76): Ms + Py = 2 Si + aQz + Phl
77): 45 Cd + 30 Ms + 14 St = 28 W + 190 Si + 30 Phl + 28 fCd

Table 9 (continued)

78): 74 Si + 22 Py + 20 Pg + 20 fCd = 20 Ab + 33 Cd + 10 St
79): 4 W + 22 Si + 6 Py + 4 fCd = 9 Cd + 2 St
80): Alm + Phl = Py + Ann
81): 12 Ab + 5 Alm + 13 Ms + 6 St = 60 Si + 12 Pg + 13 Ann
82): 17 Alm + 25 Ms + 6 St = 12 W + 96 Si + 25 Ann
83): 60 Si + 12 Pg + 13 Gr + 8 Alm = 12 Ab + 39 An + 6 St
84): 12 W + 96 Si + 25 Gr + 8 Alm = 75 An + 6 St
85): 60 Si + 12 Pg + 5 Gr + 8 Ann = 12 Ab + 15 An + 8 Ms + 6 St
86): 12 W + 96 Si + 17 Gr + 8 Ann = 51 An + 8 Ms + 6 St
87): 7 Py + 5 Ms + 2 Ann = 3 fCd + 7 Phl + 6 Si
88): 4 Si + 5 aQz + 2 Py + 2 Ann = 3 fCd + 2 Phl
89): 4 W + 22 Si + 6 Py + 6 Ann = 5 fCd + 6 Phl + 2 St
90): 21 Si + 8 Py + 25 Pg + 8 Ann = 25 Ab + 8 Phl + 6 St + 13 W
91): 60 Si + 8 Py + 12 Pg + 13 Gr + 8 Ann = 12 Ab + 39 An + 8 Phl + 6 St
92): 12 W + 96 Si + 8 Py + 25 Gr + 8 Ann = 75 An + 8 Phl + 6 St

Table 10

Reaction List for Sample RM 2

Assemblages on the left are stable on the:
high side of the Y-axis variable, or the
high side of the X-axis variable for vertical reactions

1): 2 Ann + 8 Pg + 15 aQz = 8 W + 2 Ms + 3 fCd + 8 Ab
2): aQz + Pg = Ab + Si + W
3): 10 Ab + 5 aQz + 2 St + 6 W = 10 Pg + 4 fCd
4): 8 Si + 7 aQz + 2 Ann = 3 fCd + 2 Ms
5): 3 fCd + 2 Ms + 7 Pg = 7 W + 15 Si + 2 Ann + 7 Ab
6): 16 Ab + 6 Ann + 65 aQz + 8 St = 16 Pg + 6 Ms + 25 fCd
7): 10 Ann + 95 aQz + 8 St = 16 W + 10 Ms + 31 fCd
8): 4 Ab + 11 aQz + 2 St = 6 Si + 4 Pg + 4 fCd
9): 4 fCd + 15 Pg = 11 W + 2 St + 5 Si + 15 Ab
10): 15 aQz + 2 St = 4 W + 10 Si + 4 fCd
11): 28 Ab + 5 fCd + 22 Ms + 14 St = 130 Si + 28 Pg + 22 Ann
12): 12 Ab + 8 Ms + 5 aQz + 6 St = 50 Si + 12 Pg + 8 Ann
13): 17 fCd + 30 Ms + 14 St = 28 W + 190 Si + 30 Ann
14): 8 Ms + 17 aQz + 6 St = 12 W + 62 Si + 8 Ann

Table 11

Reaction List for Sample RM 3

Assemblages on the left are stable on the:
high side of the Y-axis variable, or the
high side of the X-axis variable for vertical reactions

1): Gr + 2 Pg + 3 aQz = 2 W + 3 An + 2 Ab
2): Ann + 2 Pg + 3 aQz = 2 W + Ms + Alm + 2 Ab
3): Phl + Alm = Ann + Py
4): aQz + Pg = Ab + Si + W
5): 2 Si + aQz + Gr = 3 An
6): W + 3 Si + Gr + Ab = 3 An + Pg
7): 2 Pg + Phl + 3 aQz = 2 W + Py + Ms + 2 Ab
8): Alm + Ms = 2 Si + aQz + Ann
9): Alm + Ms + Pg = W + 3 Si + Ann + Ab
10): Py + Ms + Gr = 3 An + Phl
11): Py + Ms = Phl + aQz + 2 Si
12): Py + Pg + Ms = Ab + Phl + 3 Si + W

Table 12

Reaction list for Sample RM 4

Assemblages on the left are stable on the:
high side of the Y-axis variable, or the
high side of the X-axis variable for vertical reactions

1): 8 Pg + 2 Phl + 15 aQz = 8 W + 2 Ms + 3 Cd + 8 Ab
2): aQz + Pg = Ab + Si + W
3): 8 Si + 7 aQz + 2 Phl = 3 Cd + 2 Ms
4): 3 Cd + 2 Ms + 7 Pg = 7 W + 15 Si + 2 Phl + 7 Ab

Table 13

Reaction List for Sample RM 5

Assemblages on the left are stable on the:
high side of the Y-axis variable, or the
high side of the X-axis variable for vertical reactions

1): 2 Ann + 8 Pg + 15 aQz = 8 W + 2 Ms + 3 fCd + 8 Ab
2): aQz + Pg = Ab + Si + W
3): 10 Ab + 5 aQz + 2 St + 6 W = 10 Pg + 4 fCd
4): 8 Si + 7 aQz + 2 Ann = 3 fCd + 2 Ms
5): 3 fCd + 2 Ms + 7 Pg = 7 W + 15 Si + 2 Ann + 7 Ab
6): 16 Ab + 6 Ann + 65 aQz + 8 St = 16 Pg + 6 Ms + 25 fCd
7): 10 Ann + 95 aQz + 8 St = 16 W + 10 Ms + 31 fCd
8): 4 Ab + 11 aQz + 2 St = 6 Si + 4 Pg + 4 fCd
9): 4 fCd + 15 Pg = 11 W + 2 St + 5 Si + 15 Ab
10): 15 aQz + 2 St = 4 W + 10 Si + 4 fCd
11): 28 Ab + 5 fCd + 22 Ms + 14 St = 130 Si + 28 Pg + 22 Ann
12): 12 Ab + 8 Ms + 5 aQz + 6 St = 50 Si + 12 Pg + 8 Ann
13): 17 fCd + 30 Ms + 14 St = 28 W + 190 Si + 30 Ann
14): 8 Ms + 17 aQz + 6 St = 12 W + 62 Si + 8 Ann

Table 14

Reaction List for Sample RM 6

Assemblages on the left are stable on the:
high side of the Y-axis variable, or the
high side of the X-axis variable for vertical reactions

1): 2 Alm + 4 Pg + 9 aQz = 4 W + 3 fCd + 4 Ab
2): 2 Ann + 8 Pg + 15 aQz = 8 W + 2 Ms + 3 fCd + 8 Ab
3): Gr + 2 Pg + 3 aQz = 2 W + 3 An + 2 Ab
4): 8 Pg + 2 Phl + 15 aQz = 8 W + 2 Ms + 3 Cd + 8 Ab
5): 4 Pg + 2 Py + 9 aQz = 4 W + 3 Cd + 4 Ab
6): aQz + Pg = Ab + Si + W
7): 4 Alm + 2 Ms + 3 aQz = 3 fCd + 2 Ann
8): 3 aQz + 2 Pg + Ann = 2 Ab + Alm + Ms + 2 W
9): 2 Alm + 6 An + 3 aQz = 2 Gr + 3 fCd
10): 3 fCd + 3 Gr + 2 Pg = 2 W + 9 An + 2 Alm + 2 Ab
11): 3 Cd + 2 Alm = 3 fCd + 2 Py
12): 4 Si + 5 aQz + 2 Alm = 3 fCd
13): 5 W + 9 Si + 2 Alm + 5 Ab = 3 fCd + 5 Pg
14): 8 Ab + 6 Alm + 37 aQz + 4 St = 8 Pg + 17 fCd
15): 110 Pg + 21 fCd + 10 Alm = 110 Ab + 18 St + 74 W
16): 10 Alm + 55 aQz + 4 St = 8 W + 23 fCd
17): 3 fCd + 4 Gr + 2 Ms = 3 aQz + 12 An + 2 Ann
18): 3 fCd + 5 Gr + 2 Ms + 2 Pg = 2 W + 15 An + 2 Ann + 2 Ab
19): 3 Cd + 2 Ann = 3 fCd + 2 Phl
20): 8 Si + 7 aQz + 2 Ann = 3 fCd + 2 Ms
21): 3 fCd + 2 Ms + 7 Pg = 7 W + 15 Si + 2 Ann + 7 Ab
22): 16 Ab + 6 Ann + 65 aQz + 8 St = 16 Pg + 6 Ms + 25 fCd
23): 10 Ann + 95 aQz + 8 St = 16 W + 10 Ms + 31 fCd
24): 3 Cd + 4 Gr + 2 Ms = 3 aQz + 2 Phl + 12 An
25): 6 An + 2 Py + 3 aQz = 2 Gr + 3 Cd
26): 3 Cd + 3 Gr + 2 Pg = 2 W + 2 Py + 9 An + 2 Ab
27): 2 Si + aQz + Gr = 3 An
28): W + 3 Si + Gr + Ab = 3 An + Pg
29): 3 aQz + 4 Py + 2 Ms = 3 Cd + 2 Phl
30): 2 Pg + Phl + 3 aQz = 2 W + Py + Ms + 2 Ab
31): 8 Si + 7 aQz + 2 Phl = 3 Cd + 2 Ms
32): 3 Cd + 2 Ms + 7 Pg = 7 W + 15 Si + 2 Phl + 7 Ab
33): 10 Phl + 95 aQz + 8 St = 16 W + 10 Ms + 16 fCd + 15 Cd
34): 4 Si + 5 aQz + 2 Py = 3 Cd
35): 5 W + 9 Si + 2 Py + 5 Ab = 3 Cd + 5 Pg
36): 10 Py + 110 Pg + 36 fCd = 110 Ab + 15 Cd + 18 St + 74 W
37): 10 Py + 55 aQz + 4 St = 8 W + 8 fCd + 15 Cd
38): 4 Ab + 11 aQz + 2 St = 6 Si + 4 Pg + 4 fCd

Table 14 (continued)

39): 4 fCd + 15 Pg = 11 W + 2 St + 5 Si + 15 Ab
40): 15 aQz + 2 St = 4 W + 10 Si + 4 fCd
41): 7 Alm + 5 Ms = 6 Si + 3 fCd + 5 Ann
42): Alm + Ms = 2 Si + aQz + Ann
43): Alm + Ms + Pg = W + 3 Si + Ann + Ab
44): 12 Pg + 37 Ms + 65 Alm = 12 Ab + 37 Ann + 30 fCd + 6 St
45): 12 Pg + 17 Ms + 25 Alm = 12 Ab + 17 Ann + 30 aQz + 6 St
46): 12 W + 23 Ms + 31 Alm = 23 Ann + 48 aQz + 6 St
47): 6 Si + 5 Gr + 3 fCd = 2 Alm + 15 An
48): 12 Ab + 30 fCd + 37 Gr + 6 St = 12 Pg + 111 An + 28 Alm
49): 48 fCd + 55 Gr + 6 St = 12 W + 165 An + 40 Alm
50): 20 W + 6 St + 7 Gr + 32 Ab = 8 Alm + 21 An + 32 Pg
51): 24 Ab + 34 Py + 111 aQz + 12 St = 24 Pg + 51 Cd + 16 Alm
52): 46 Py + 165 aQz + 12 St = 24 W + 69 Cd + 16 Alm
53): 74 Si + 20 Pg + 22 Alm = 20 Ab + 13 fCd + 10 St
54): 12 Ab + 13 aQz + 6 St = 34 Si + 12 Pg + 8 Alm
55): 4 W + 22 Si + 6 Alm = 5 fCd + 2 St
56): 21 Si + 25 Pg + 8 Alm = 25 Ab + 6 St + 13 W
57): 25 aQz + 6 St = 12 W + 46 Si + 8 Alm
58): 6 Si + 2 Ms + 7 Gr + 3 fCd = 2 Ann + 21 An
59): 48 fCd + 95 Gr + 40 Ms + 6 St = 12 W + 285 An + 40 Ann
60): 28 Ab + 5 fCd + 22 Ms + 14 St = 130 Si + 28 Pg + 22 Ann
61): 17 fCd + 30 Ms + 14 St = 28 W + 190 Si + 30 Ann
62): 8 Ms + 17 aQz + 6 St = 12 W + 62 Si + 8 Ann
63): Py + Ms + Gr = 3 An + Phl
64): 3 Cd + 7 Gr + 2 Ms + 6 Si = 2 Phl + 21 An
65): 3 Cd + 5 Gr + 6 Si = 2 Py + 15 An
66): 12 Ab + 42 Cd + 37 Gr + 6 St = 28 Py + 12 Pg + 12 fCd + 111 An
67): 60 Cd + 55 Gr + 6 St = 12 W + 40 Py + 12 fCd + 165 An
68): 28 Si + 4 Pg + 11 Gr + 4 fCd = 4 Ab + 33 An + 2 St
69): 4 W + 40 Si + 15 Gr + 4 fCd = 45 An + 2 St
70): 7 Py + 5 Ms = 3 Cd + 5 Phl + 6 Si
71): Ms + Py = 2 Si + aQz + Phl
72): Ms + Pg + Py = W + 3 Si + Phl + Ab
73): 45 Cd + 30 Ms + 14 St = 28 W + 190 Si + 30 Phl + 28 fCd
74): 74 Si + 22 Py + 20 Pg + 20 fCd = 20 Ab + 33 Cd + 10 St
75): 4 W + 22 Si + 6 Py + 4 fCd = 9 Cd + 2 St
76): Alm + Phl = Py + Ann

Table 14 (continued)

77): 12 Ab + 5 Alm + 13 Ms + 6 St = 60 Si + 12 Pg + 13 Ann
78): 17 Alm + 25 Ms + 6 St = 12 W + 96 Si + 25 Ann
79): 60 Si + 12 Pg + 13 Gr + 8 Alm = 12 Ab + 39 An + 6 St
80): 12 W + 96 Si + 25 Gr + 8 Alm = 75 An + 6 St
81): 222 Si + 26 Py + 60 Pg + 40 Alm = 60 Ab + 39 Cd + 30 St
82): 3 aQz + 2 Py + 6 An + 2 Ann = 3 fCd + 2 Gr + 2 Phl
83): 12 W + 96 Si + 17 Gr + 8 Ann = 51 An + 8 Ms + 6 St
84): 4 Si + 5 aQz + 2 Py + 2 Ann = 3 fCd + 2 Phl
85): 3 fCd + 5 Gr + 2 Phl + 6 Si = 2 Py + 15 An + 2 Ann
86): 4 W + 22 Si + 6 Py + 6 Ann = 5 fCd + 6 Phl + 2 St
87): 21 Si + 8 Py + 25 Pg + 8 Ann = 25 Ab + 8 Phl + 6 St + 13 W
88): 60 Si + 8 Py + 12 Pg + 13 Gr + 8 Ann = 12 Ab + 39 An + 8 Phl + 6 St
89): 12 W + 96 Si + 8 Py + 25 Gr + 8 Ann = 75 An + 8 Phl + 6 St

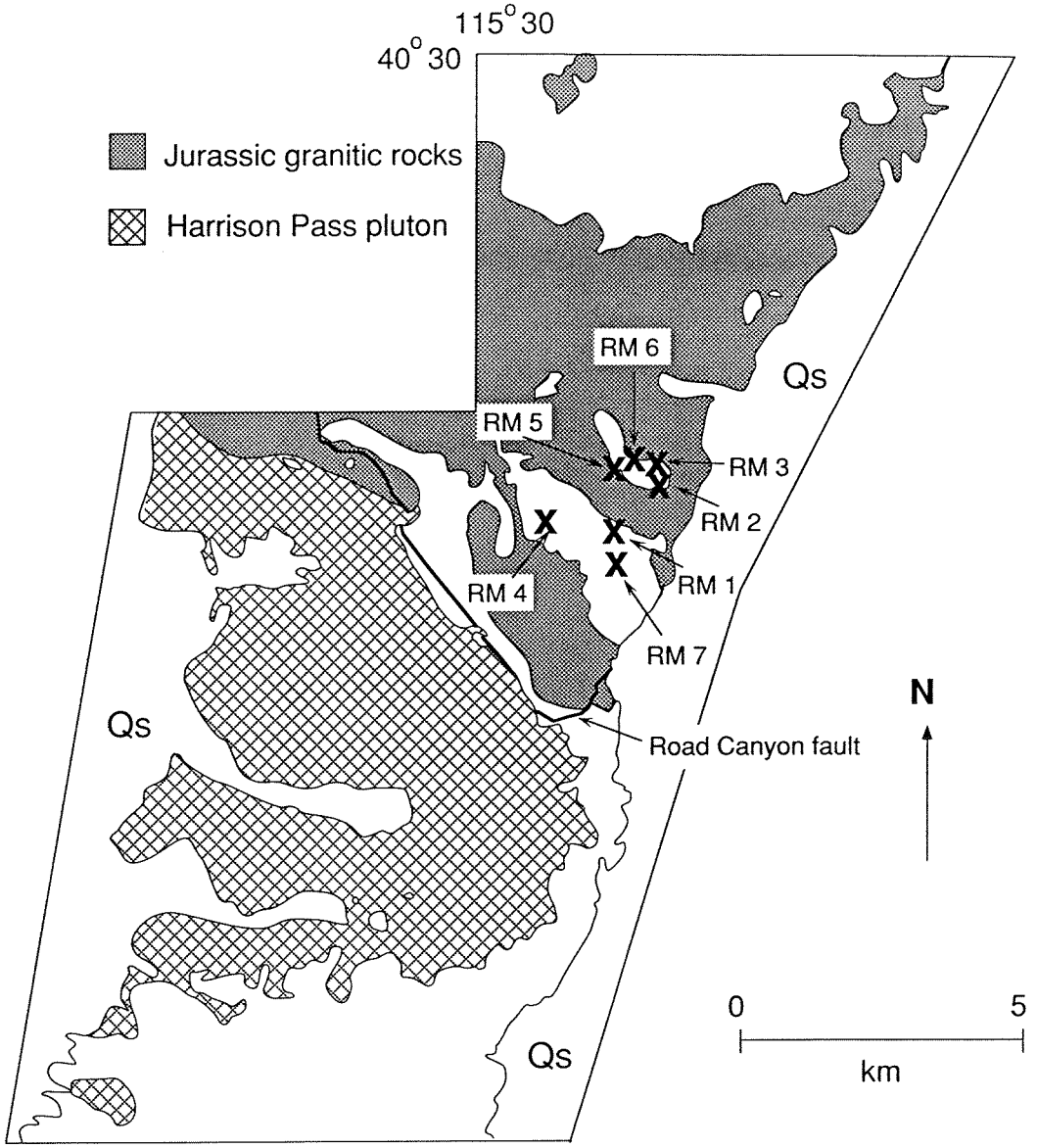

Figure 1. Location of thermobarometry samples in the central Ruby Mountains.

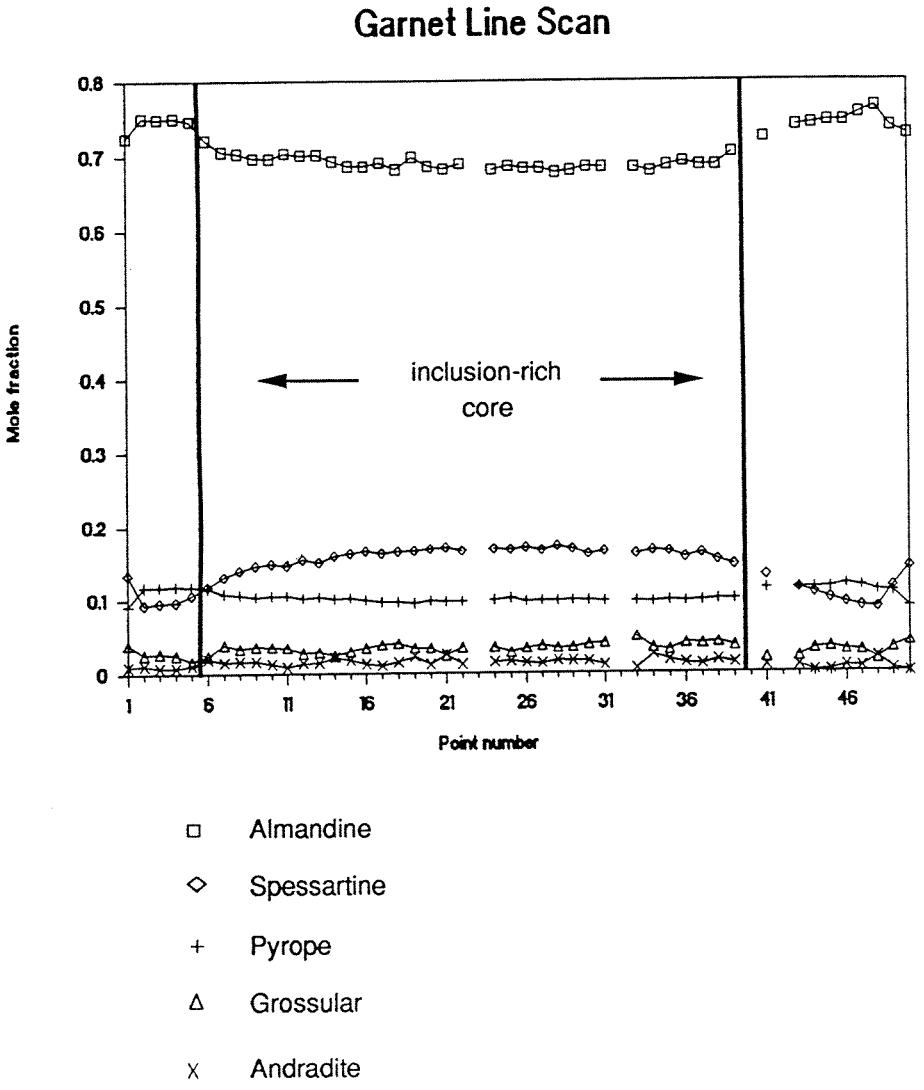

Figure 2. Garnet line scan showing the compositional break between the inclusion-rich core and inclusion-free rim of the garnet.

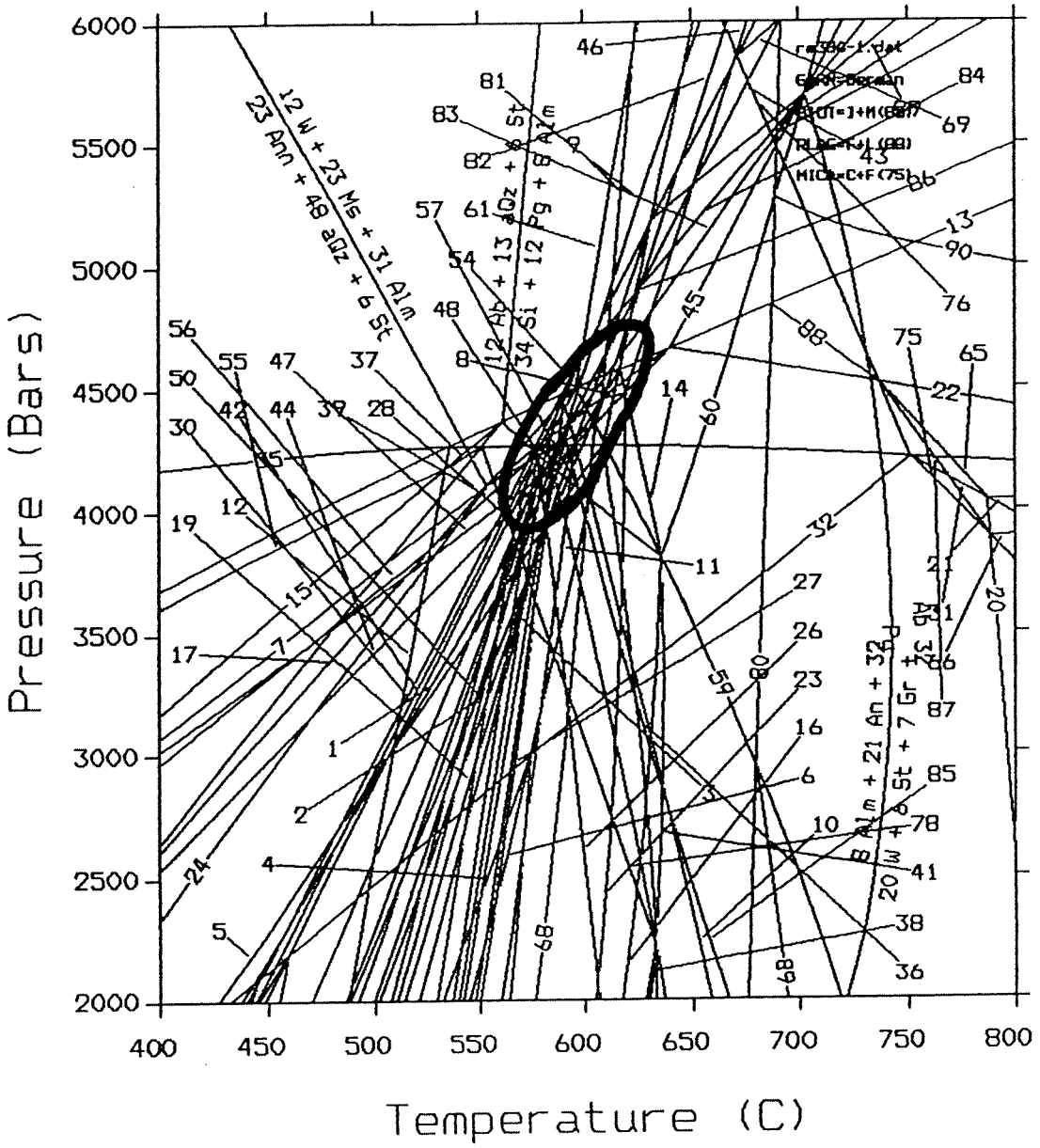

Figure 3. Phase diagram for sample RM 1.

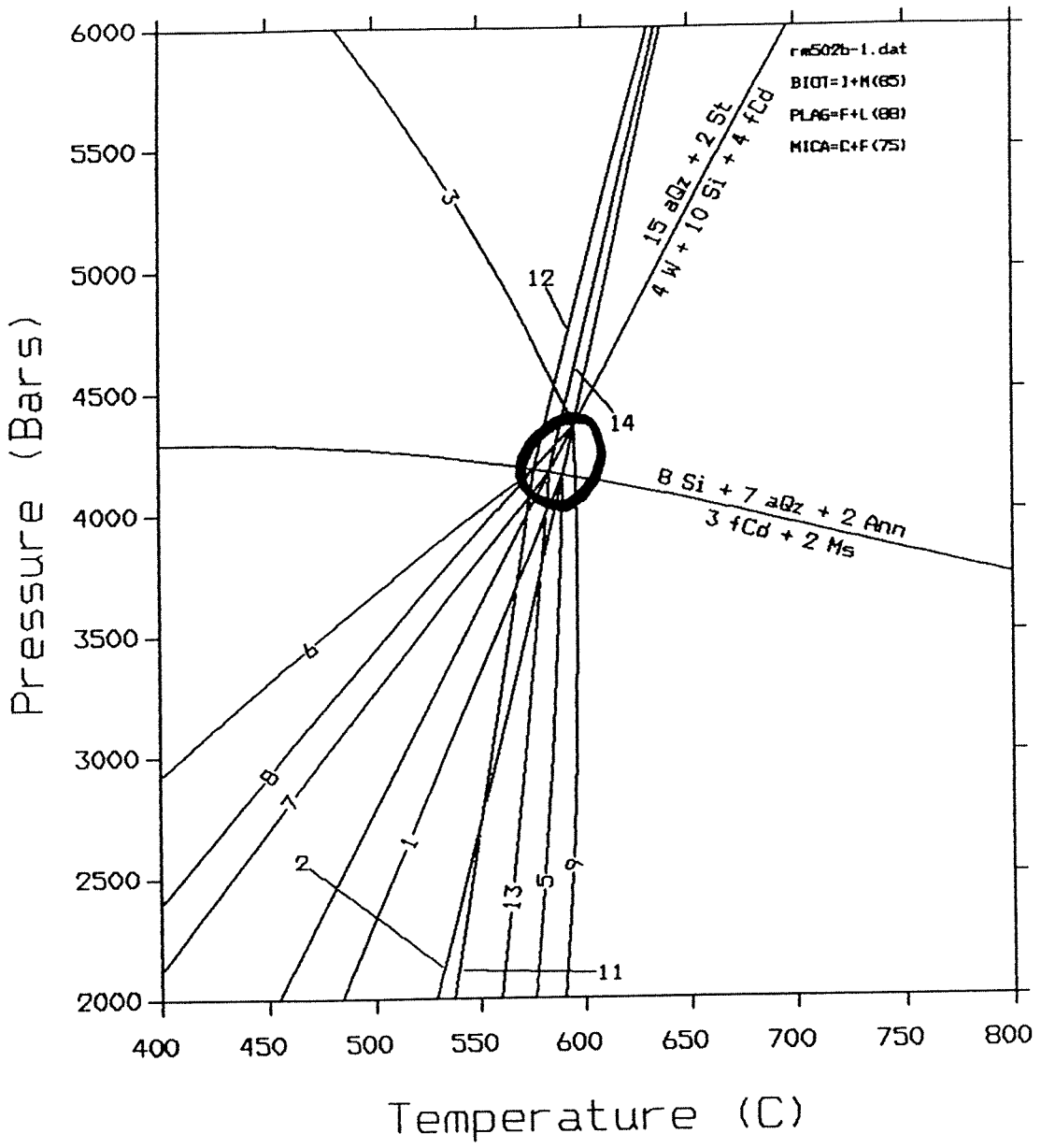

Figure 4. Phase diagram for sample RM 2.

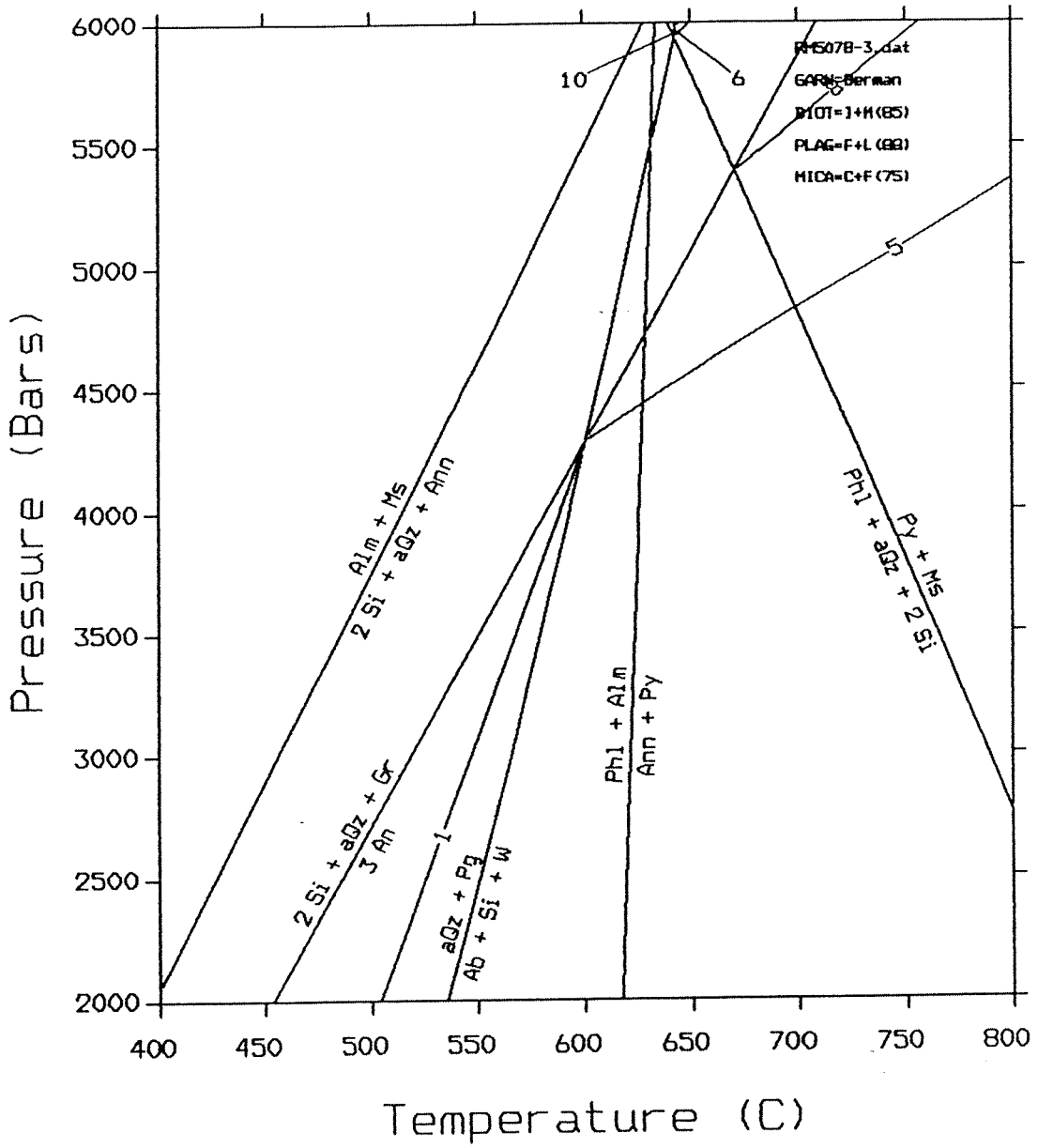

Figure 5. Phase diagram for sample RM 3.

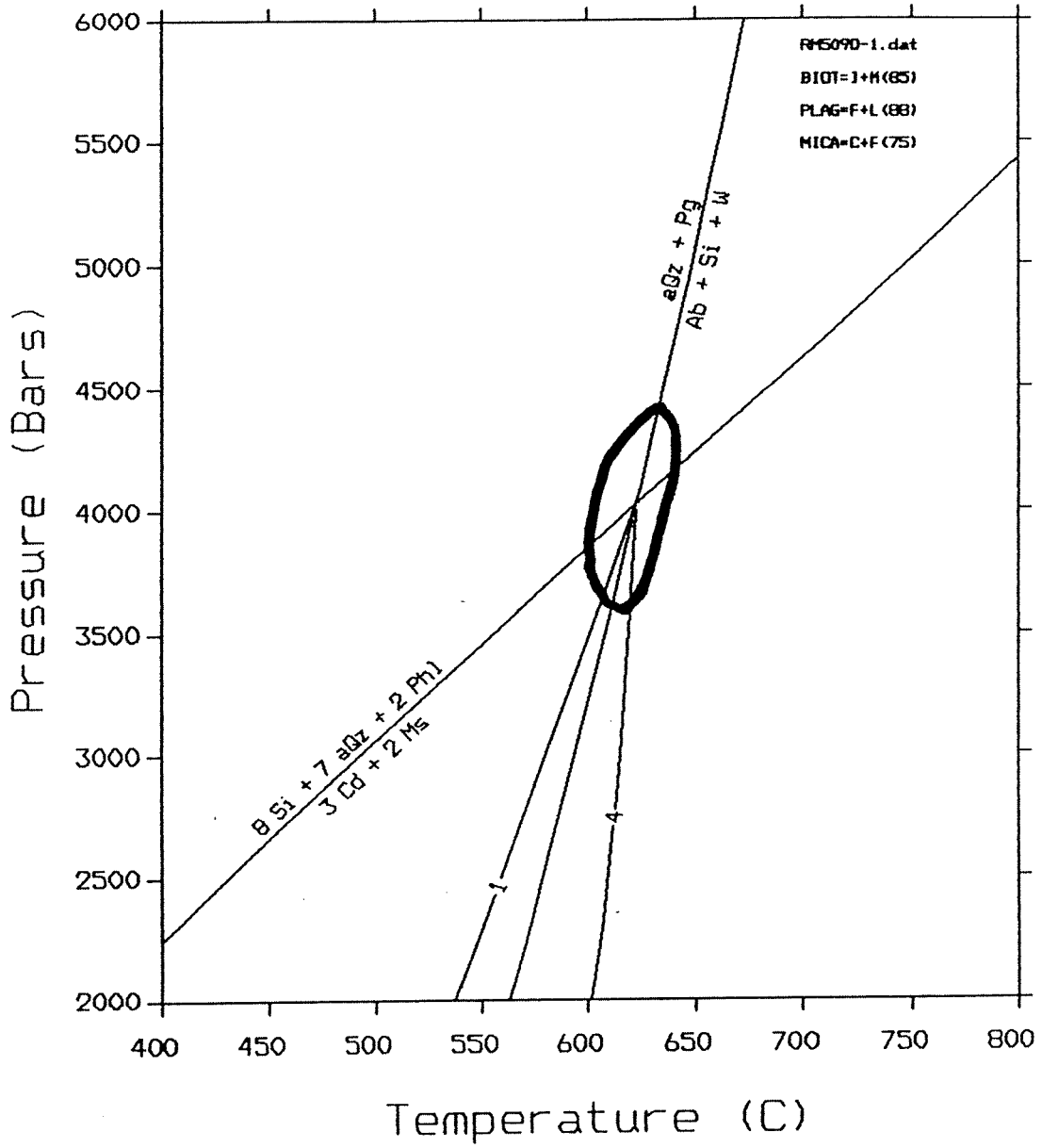

Figure 6. Phase diagram for sample RM 4.

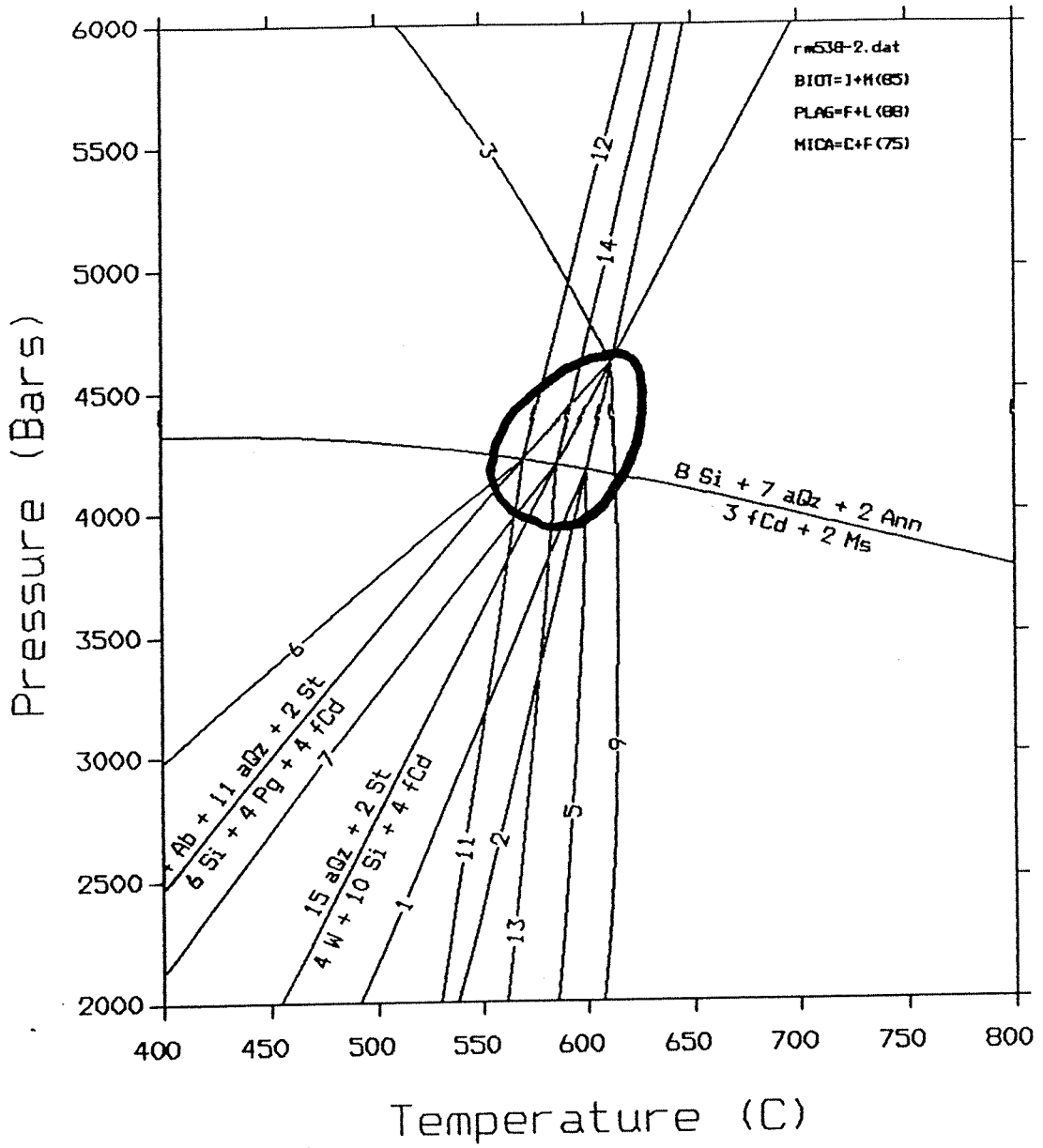

Figure 7. Phase diagram for sample RM 5.

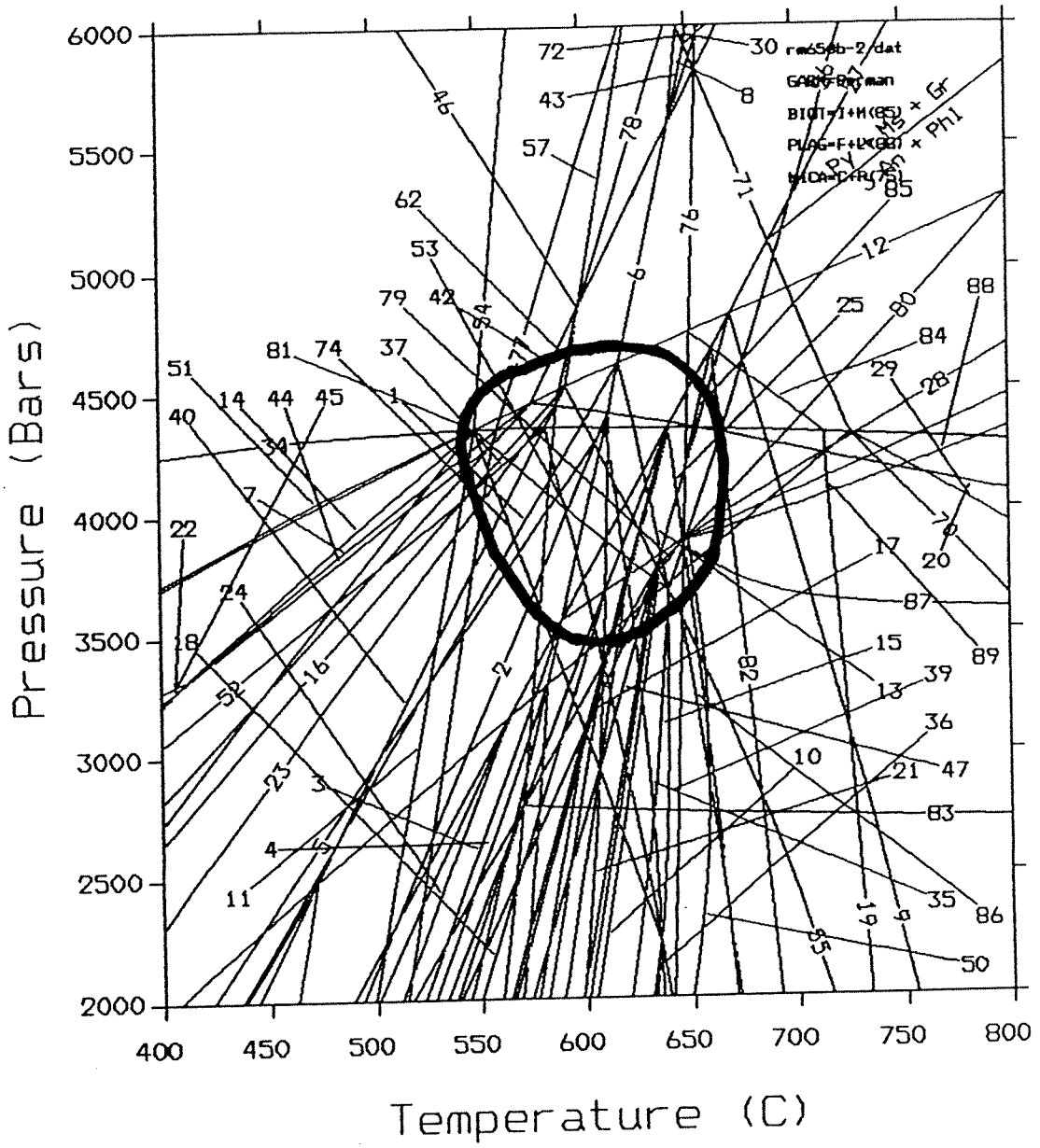

Figure 8. Phase diagram for sample RM 6.

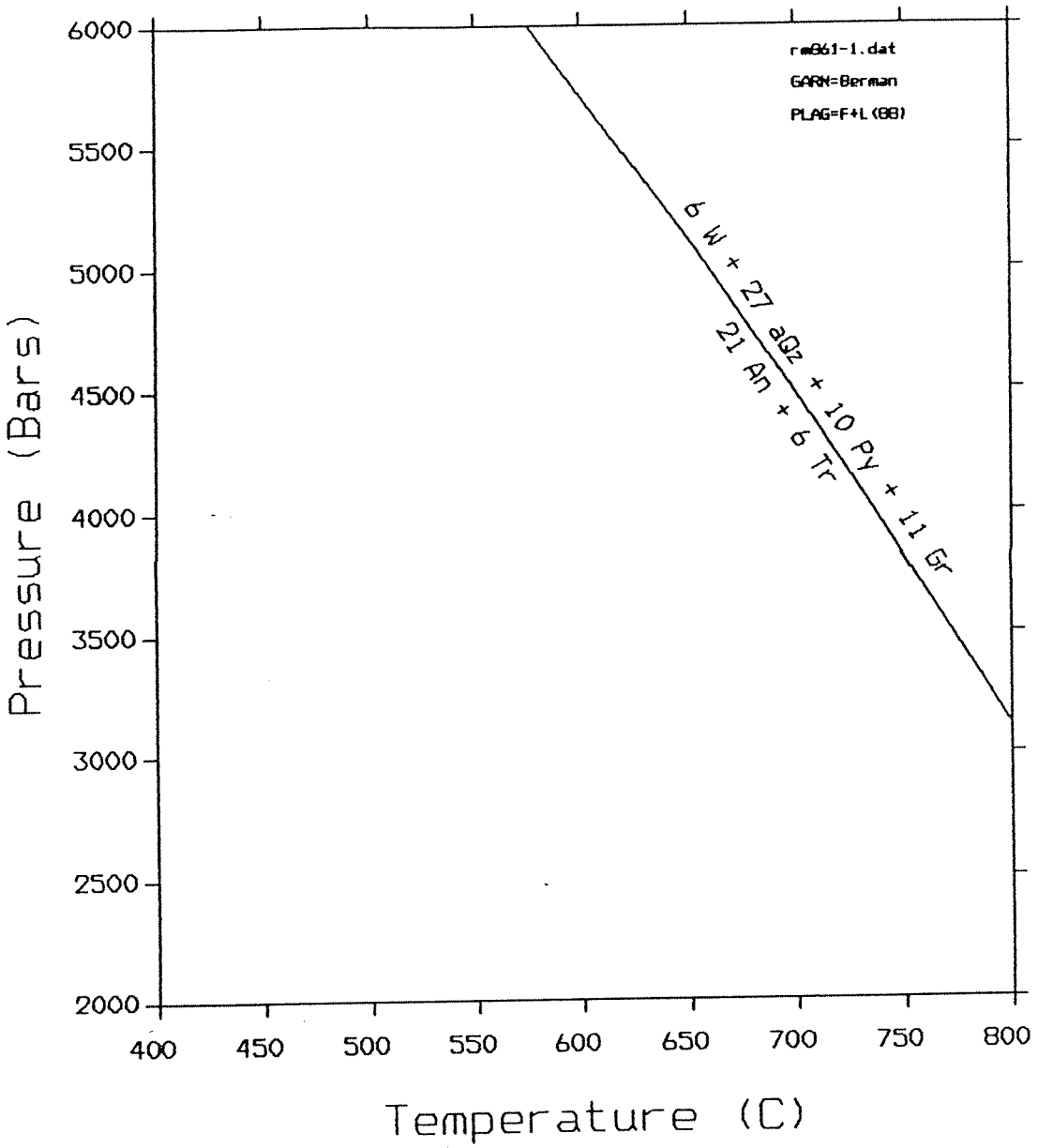

Figure 9. Phase diagram for sample RM 7.

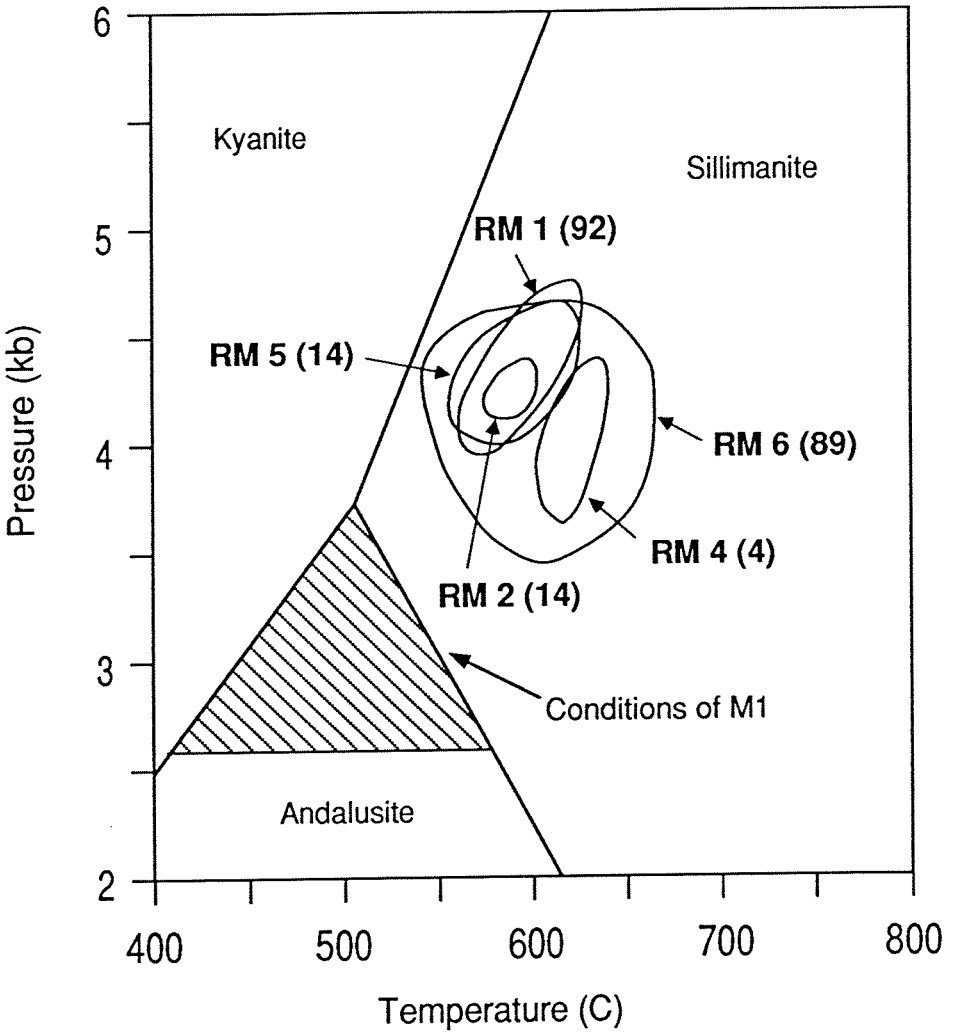

Figure 10. Diagram showing the positions of the invariant point clusters relative to one another in pressure-temperature space. The clusters together define the conditions of M_2 metamorphism, approximately 3.5-4.7 kb and 540-660° C. The position of M_1 conditions is shown for comparison.